Journal Homepage: http://ijcpe.uobaghdad.edu.iq
Iraqi Journal of Chemical and Petroleum Engineering
Vol. 26 No. 4 (December 2025) 133 – 150
EISSN: 2618-0707, PISSN: 1997-4884

Green synthesis of NiO nanoparticles with activated carbon from Ficus carica leaf and extract for malachite green removal

Raghad Mohammed Hadi [a, *], Sami D. Salman [a]

a Biochemical Engineering Department, Al-Khwarizmi College of Engineering, University of Baghdad, Baghdad 47024, Iraq

Abstract

The green synthesis of nanoparticles and activated carbon has attracted researchers' interest due to its rapid, cost-effective, sustainable, and environmentally friendly nature. In this paper, the synthesis of activated carbon (AC) and nickel oxide nanoparticles (NiO-NPs) from Ficus carica leaf and their extracts for the removal of malachite green from aqueous solutions. activated carbon (AC) was synthesized from Ficus carica leaves using a pyro-carbonic acid microwave method. In contrast, nickel oxide nanoparticles were produced using leaf extracts as a reducing and stabilizing agent. The manufactured activated carbon and NiO nanoparticles were characterized by Brunauer-Emmett-Teller analysis, scanning electron microscopy with energy-dispersive X-ray spectroscopy, X-ray diffraction, and Fourier transform infrared spectroscopy. The influence of various factors, including malachite green concentration, pH, contact time, and dosages of NiO, AC, and NiO/AC, was examined using Response Surface Methodology (RSM) in Design-Expert (13 Stat-Ease). the optimal parameters for achieving maximum removal efficiency of malachite green dye were determined to be an initial concentration of 150 mg/L, pH of 4, a contact period of 120 minutes, and an adsorbent dosage of 0.25 g/L, resulting in removal efficiencies of 97.9202%, 98.8932%, and 99.9776%, respectively. The equilibrium adsorption data were analyzed using the Langmuir, Freundlich, and pseudo-first- and second-order kinetic models. the results indicated that the Freundlich isotherm and pseudo-second-order kinetic models were the most effective in representing the equilibrium adsorption data.

Keywords: Ficus carica leaf; green synthesis nanoparticles; activated carbon; malachite green.

Received on 16/06/2025, Received in Revised Form on 08/08/2025, Accepted on 08/08/2025, Published on 30/12/2025

https://doi.org/10.31699/IJCPE.2025.4.12

1- Introduction

Currently, an eco-friendly and pure environment is regarded as a prominent subject in academic research and industry.one of the primary environmental pollutants is industrial effluents containing highly colored dyes with substantial quantities of organic solids [1]. malachite green, as a coloring dye, has various industrial applications, including the dyeing of silk, textiles, leather, plastics, and paper, as well as serving as a fungal and parasitic insecticide in aquaculture [2-4]. Despite its various applications in coloring, malachite green is a toxic metal ion detrimental to aquatic organisms due to its mutagenic and carcinogenic properties [5, 6]. various practical strategies and solutions have been implemented to generate more sustainable water resources, including coagulation and flocculation [7], oxidation or ozonation [8, 9], membrane separation [10], biodegradation [11], adsorption [12, 13]. Among these methods, adsorption is a dependable technique due to its simplicity, high efficiency, and low cost [14]. activated carbon (AC) is an amorphous form of carbon that is subjected to specific treatments that create a highly intricate internal pore structure and a substantial surface area, resulting in a cost highly effective and superior adsorbent , as noted by [15]. Activated carbon features significant porosity, a considerable surface area (up to 3000 m^2/g), varied surface chemical properties, and high surface reactivity, making it an exceptionally efficient adsorbent for the removal of diverse organic and inorganic pollutants in aqueous solutions [16-18]. Coal, wood, and coconut shell are the primary carbonaceous materials employed in the industrial production of activated carbons, as stayed by [19] .However, these kinds are sometimes expensive and imported, compelling developing nations to pursue economical and accessible feedstock for the synthesis of activated carbon for industrial uses, potable water filtering, and wastewater treatment. agricultural by-products can be classified into two main categories: (I) Soft, compressible, low-density waste materials, including rice husks, sugarcane bagasse, and peanut and soybean shells; and (II) hard, dense, non-compressible agricultural by-products, such as pecan and walnut shells, along with stones from dates, apricots, or cherries. Various suitable agricultural by-products include olive cakes and olive stones. Recent studies have examined many materials as precursors for activated carbon (AC), including olive waste cakes [20], dates stones [15], tobacco stems [21], almond shells [22], corn cobs [23], waste tea [24], waste apricots [25], sawdust [26], cherry stones [27], rice bran [28], durian shells [29], herb residues [30]. In recent years, nanostructured materials have attracted significant

*Corresponding Author: Email: raghad.hadi2405m@kecbu.uobaghdad.edu.iq

attention due to their nanoscale particles, enhanced surface area, volume, quantum effects, chemical reactivity, conductivity, and lightweight characteristics [31]. These materials can be generated using hydrothermal, microemulsion, electrospray, coprecipitation, laser ablation, and sol-gel methods [32, 33]. However, these methods are quite expensive, offer minimal results, and use hazardous chemicals that harm the environment [34]. Consequently, bio-derived materials present a cost-effective and eco-friendly option for the adsorption of dyes and pollutants from wastewater effluents [35, 36]. nickel oxide is a notable metal oxide that has drawn current interest through green synthesis methods using various plant extracts for diverse applications, due to its non-toxicity, simplicity, cost-effectiveness, environmental friendliness, short reaction durations, and natural biodegradability [37-43]. The characteristics of activated carbon and NiO nanoparticles motivated the current research. In this research Ficus carica leaf was used to prepare activated carbon by pyro carbonic acid with microwave technique and Ficus carica leaf extract was used to synthesis NiO nanoparticles. The activated carbon, NiO nanoparticles, and NiO/AC were characterized by Brunauer-Emmett-Teller analysis, scanning electron microscopy with energy dispersive X-ray analysis, X-ray diffraction, and Fourier transform infrared spectroscopy. Finally, the NiO nanoparticles, activated carbon AC, and NiO/AC were used for malachite green removal from aqueous solution. Design-Expert (13 Stat-Ease) software with Response Surface Methodology (RSM) was employed to examine the influence of initial concentration, pH, contact time, and the dose of NiO, activated carbon (AC), and NiO/AC on the malachite green removal efficiency.

2- Materials and methods

2.1. Chemicals

Malachite Green (MG) dye was used as the contaminant and acquired from Sigma Aldrich. all solutions were formulated using pure water the pH of the solution was modified by the addition of 0.1 N HCl or NaOH solution. a stock solution of various concentrations was generated from a standard MG dye solution by dissolving 1 g of MG dye in 1 L of distilled water. the standard solution was diluted with distilled water to get the required dye solution concentrations (0 – 250 mg/L). the concentrations of dye were quantified using UV-visible spectroscopy (λ = 617 nm) with the calibration curve shown in Fig. 1.

2.2. Preparation of activated carbon

Ficus carica leaf were collected from the gardens of the University of Baghdad. the leaf is first cleaned with water to remove dirt and dust, then dried in the shade for 24 hours, and subsequently placed in an oven at 100°C for two hours. the leaf was ground and sorted to a particle size ranging from 720 micrometers to 1 millimeter. After that, the sample was pre-prepared and activated following the process documented by [30] .the sample was submerged with 80% H3PO4 at an impregnation ratio of 1:2 for 8 hours, subsequently filtered to remove excess acid, and then placed in a glass reactor for microwave activation at 700 watts for 20 minutes. the activated carbon was washed with hot water to remove acid residues until the pH of the wash water reached 6.5-7, after that dried at 105˚C for 24 hours, and finally grinding to the desired particle size.

2.3. Preparation of NiO-NPs

Fresh Ficus leaves were harvested, cleansed, and air-dried at room temperature subsequent to cleaning, 40 g of leaf powder was put into 400 ml of autoclaved distilled water. the solution was placed on a heated plate at 70–80 °C for 2 hours under magnetic stirrer. after cooling, the crud extract was filtered three times using Whatman filter paper, and the supernatant was collected at a pH of 6.8. the leaf extract was preserved at 4°C for subsequent research to produce NiO nanoparticles on activated carbon, 7.5 g of Ni $(NO_3)_2{\cdot}6H_2O$ was dissolved in 50 ml of water and agitated for 30 minutes at room temperature. then, 30 ml of leaf extract was incrementally added to the Ni $(NO_3)_2{\cdot}6H_2O$ solution to obtain a clear brown solution. Subsequently, the resulting sol was agitated for 4 hours using a magnetic stirrer at a constant temperature of 80 °C. Finally, a green and viscous gel was noted to remain in the dish, which was subjected to drying at 180 °C for 2 hours. The dried gel undergo calcination for 3 hours at a temperature of 300 °C to yield a greyish-black powder. Similar process was applied to prepared NiO nanoparticles using sol–gel method [44].

2.4. Preparation of (NiO-NPs) on AC

Add 0.5 g of NiO nanoparticles to 250 mL of distilled water and homogenized the solution on a magnetic mixer for 20 min. then add 5 g of the AC to the solution and blend at 500 rpm for 2 h. Finally, purified the mixture by washing and filtration with distilled water, and dried at 105 °C overnight. Then, the product was calcined at 350 °C for 4 h to obtain final composite adsorbent material. similar process was applied to prepared Ag/ZNO-AC composite photocatalyst using certain quantity of Ag/ZNO with AC [45].

3- Result and discussion

3.1. Brunaure, Emmett, and teller (BET)

The liquid nitrogen adsorption-desorption isotherm was using to calculated the specific surface area of the raw material, activated carbon, and AC/NiO. the specific surface area, particle size, and pore volume were calculated using the Brunauer-Emmett-Teller (BET) method with a HORIBA SA-900 series analyzer from the USA, as presented in Table 1.

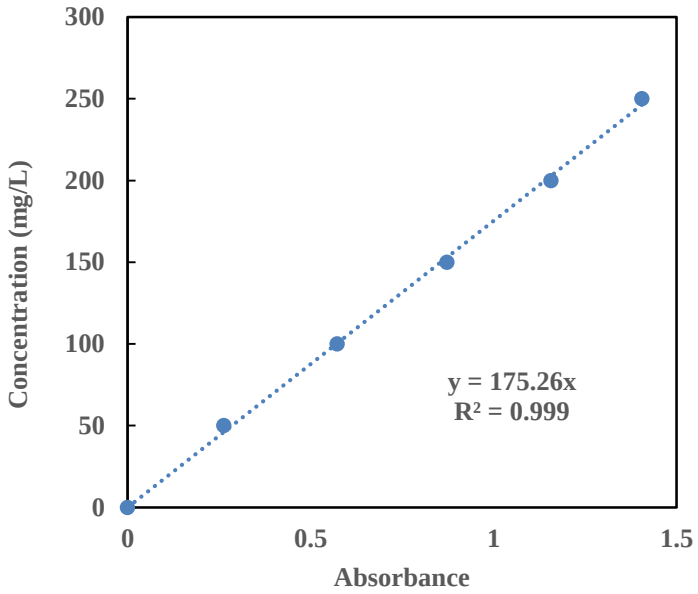

Fig. 1. Calibration curve for MG concentration

Table 1. BET analysis of activated carbon

Sample	surface area [m^2 /g]	Average pore diameter [nm]	Total pore volume [cm^3 /g]
Ficus carica	0.0193	5.6405	0.012645
activated carbon	904.5264	2.38746	0.539879
AC/NIO	961.6142	2.35487	0.5661

The BET surface areas of Ficus carica leaf-derived activated carbons were significantly elevated, attributed to the evaporation and breakdown of water and volatile components, which create fissures and porosities on the activated carbon's surface during production. similarly, the BET surface areas of AC/NiO increased to 961.6142 m^2/g due to the presence of NiO nanoparticles on the activated carbon surface, which possesses a higher surface-to-volume ratio than activated carbon. Similar results were found for the surface modification of activated carbon using silver nanoparticles [46].

3.2. Scanning electron microscopy (SEM) with EDS

The surface morphology and topographical features were analyzed using a scanning electron microscope (SEM) The resulting images are three-dimensional and precisely represent the surface contour. The Energy Dispersive X-ray Spectrophotometer is used to analyze the elemental composition of the precursors (EDS). Fig. 2, Fig. 3, and Fig. 4 illustrate the surface morphology of Ficus carica leaf, activated carbon (AC), and nickel oxide nanoparticles (NiO-NPs) on AC. Fig. 2 illustrates that the surface of the Ficus carica leaf is soft and uniform, exhibiting a small number of pores. in contrast, Fig. 3 illustrates that the activated carbon surface is heterogeneous, characterized by a porous structure with varying shapes and sizes. this phenomenon may occur due to the decomposition and volatilization of the activating agent and non-carbonaceous materials during the activation and carbonization processes [47]. Fig. 4. show a little alteration in the surface morphology of the composite activated carbon. this discovery may be ascribed to surface coverage and pore volume obstruction caused by metal oxide particles formed on the surface [48]. the pores formed in the activated carbon enhance the adsorption of diesel oil due to the diffusion and reactivity of H_3PO_4 with cellulose compounds, resulting in the production of phosphate ester. as a result, the phosphate ester decomposed, creating micropores during the microwave activation. Fig. 5, Fig. 6, and Fig. 7 illustrate the elemental compositions of the precursor and activated carbon as determined by spectroscopic (EDS) techniques. the results showed that chemical activation and microwave carbonization increased the carbon content from 48.41% in Ficus carica to 84.30% in the generated activated carbon (see Table 2, Table 3, and Table 4).The elemental compositions altered due to the increase of activated carbon [49]. In addition, the elemental compositions of composite activated carbon showed a significant reduction in carbon content attributable to the presence of metal oxides on the surface resulting from the thermal precipitation of NiO on activated carbon [50].

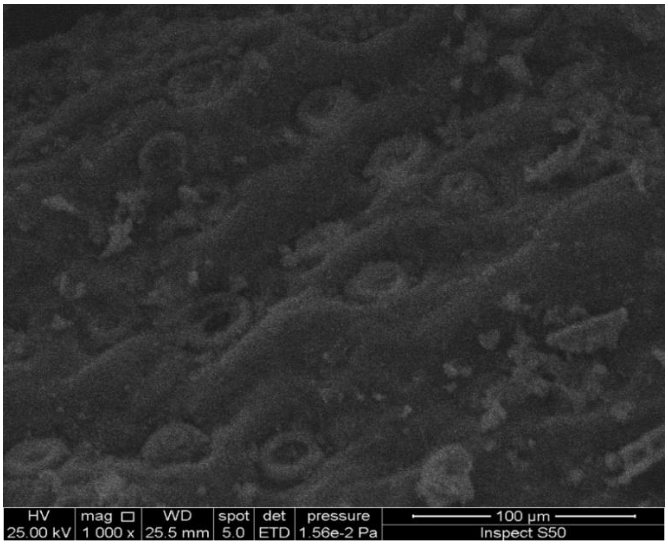

Fig. 2. Scanning Electron Microscope (SEM) image of Ficus carica leaf

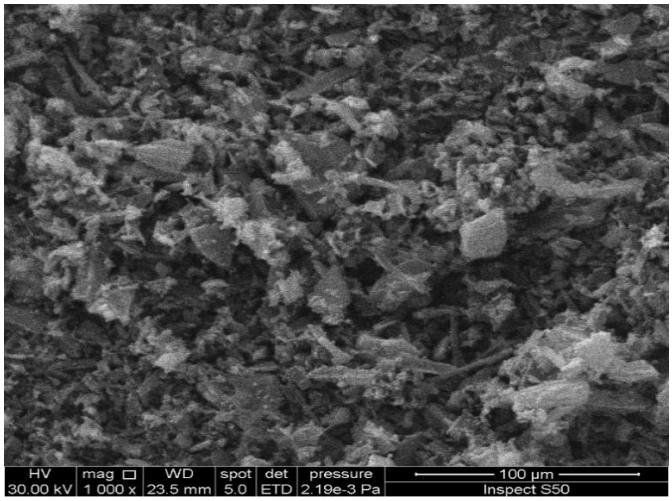

Fig. 3. Scanning Electron Microscope (SEM) for AC

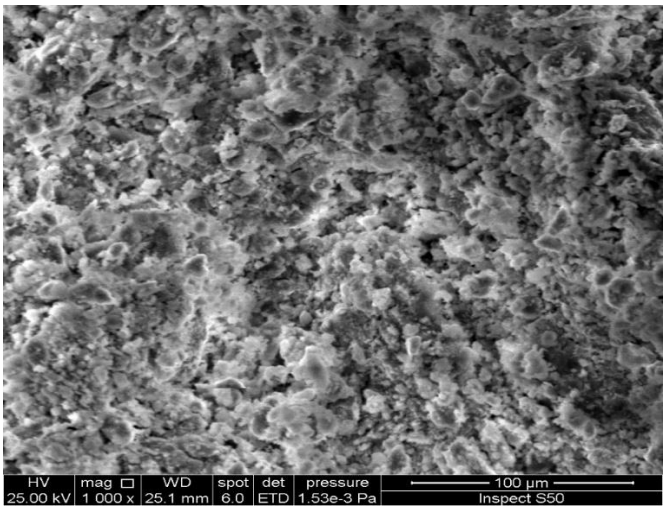

Fig. 4. Scanning Electron Microscopy of NiO/Activated Carbon

3.3. Fourier Transform Infrared Spectroscopy (FTIR)

Fourier Transform Infrared Spectroscopy IR Affinity-1 Shimadzu, Japan was used to determine the functional groups present on the surfaces of Ficus carica leaf, activated carbons, and NiO/AC, as illustrated in Fig. 8, Fig. 9, and Fig. 10. The FTIR spectra for activated carbon derived from Ficus carica leaf, across the wavelength

range of 4000 to 450 cm^{-1}, are illustrated in Fig. 8. The Ficus carica exhibits several peaks that indicate the complex characteristics of the raw material. The peaks in the range of 3500-4000 cm^{-1} were attributed to the OH stretching vibration, resulting from the presence of alcohols, chemisorbed water, and phenols [51]. the absorption peaks in the range of 2500-3500 cm^{-1} are attributed to -CH, $-CH_2$, and other saturated aliphatic groups. Similarly, the peak at 2300 cm^{-1} corresponds to the OH band, while the peaks at 1500-2000 cm^{-1} indicate the presence of COOH. The peaks within the range of 1000-1500 cm^{-1} indicate aldehyde C=O and phenol C=C groups, while the peaks between 500-1000 cm^{-1} relate to the vibrational bending of aromatic compounds. [52, 53]. in addition, several peaks vanished due to activation, while others emerged as a result of new bond synthesis in activated carbon. The peaks identified between 3500-4000 cm^{-1} are attributed to the oscillation of the stretching bond of free hydrogen associated with −OH groups [51]. the absorption bands within the range of 2500-3000 cm^{-1} correspond to the C-O stretching vibration bond of carbon dioxide or carbon monoxide. the peak in the range of 2000-2500 cm^{-1} refers to the bond stretching vibrations of alkynes (C≡C),while the peaks between 1500-2000 cm^{-1} pertain to the stretching vibrations of C=C [54]. The peaks between 1000-1500 cm^{-1} are attributed to the symmetric and antisymmetric stretching of (N=O) and C-O-C bonds [55]. The peaks at 3700–3200 cm^{-1} correspond to the -OH bond stretching on the activated carbon surface. the peak between 1000-1500 cm^{-1} corresponds to the vibrational mode of H–OH, while HOH bending was seen between 1600-2000 cm^{-1} [56]. A high stretching at 490 cm^{-1} is linked to the heterogeneous nucleation of the Ni–O bond, indicating that the composite activated carbon was successfully produced [57].

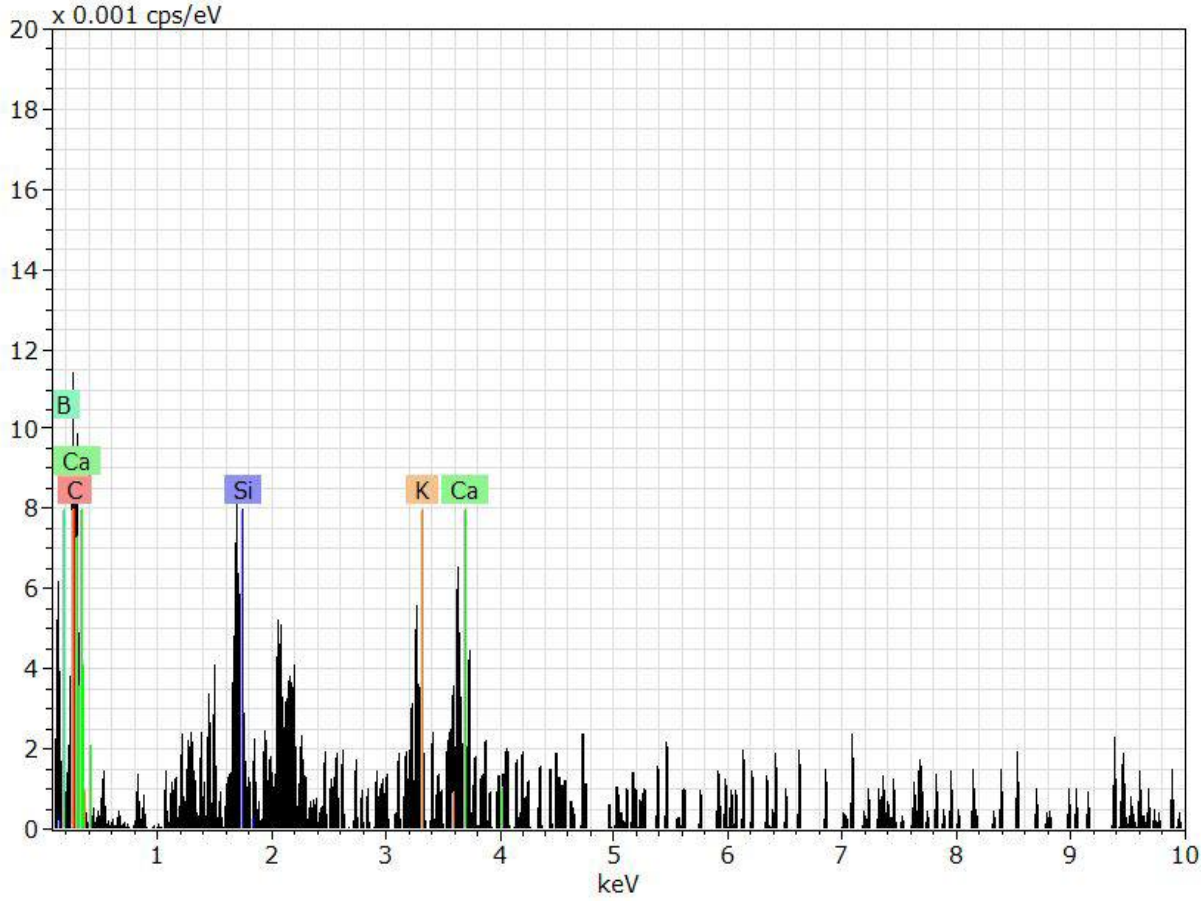

Fig. 5. Energy Dispersive Spectroscopy (EDS) for Ficus carica leaf

Table 2. Elemental composition of Ficus carica leaf

Element	Weight %	Atomic %	Weight % Error
C	48.41	54.98	8.48
Ni	15.75	2.00	0.00
Si	5.84	3.03	0.23
P	17.26	13.56	0.23
N	12.74	26.43	0.48
Total	100.00	100.00	

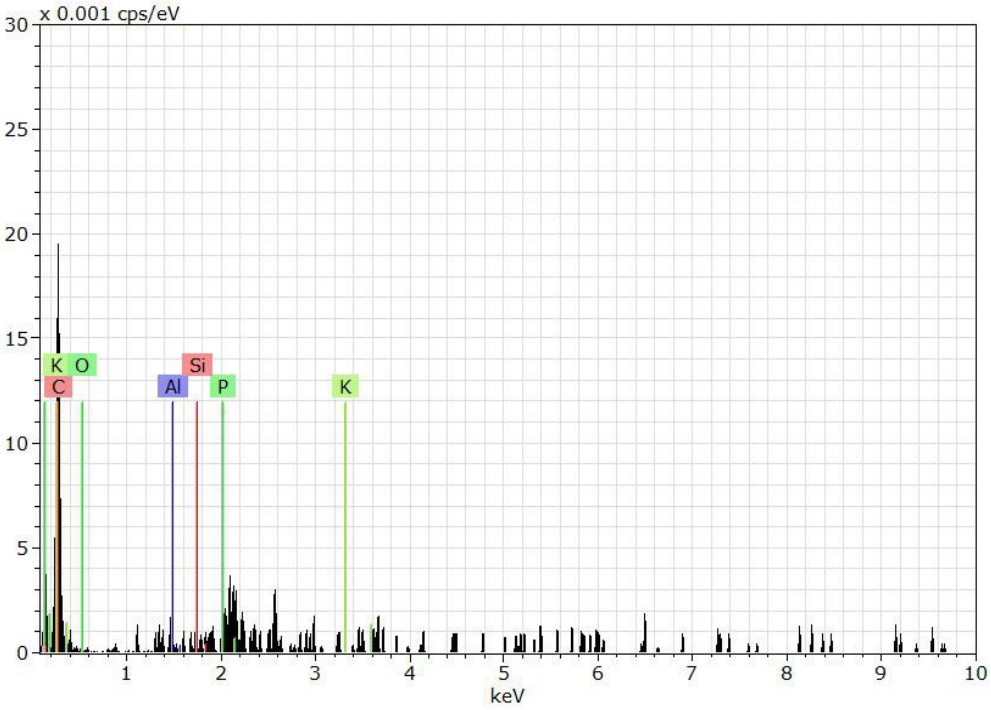

Fig. 6. Energy Dispersive Spectroscopy for Activated Carbon

Table 3. Elemental composition of activated carbon

Element	Weight %	Atomic %	Weight % Error
C	84.30	96.53	10.55
Ca	6.29	0.71	0.51
Al	4.37	2.23	0.41
Ba	3.73	0.37	0.47
K	1.31	0.16	0.23
Total	100.00	100.00	

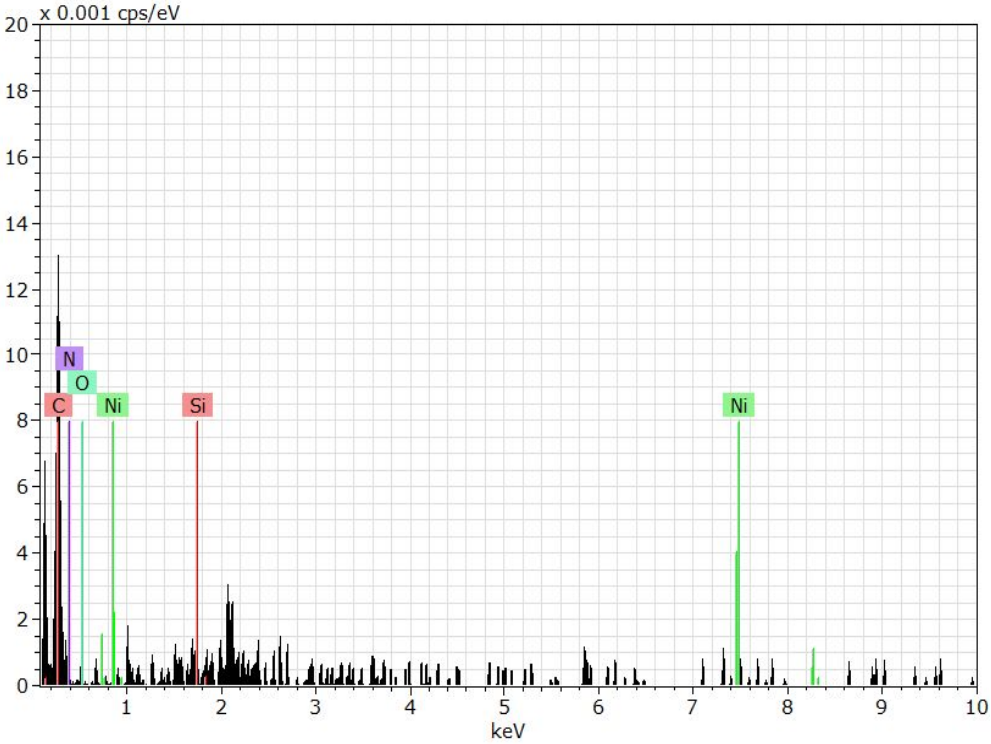

Fig. 7. Energy Dispersive Spectroscopy for Nickel Oxide/Activated Carbon

Table 4. Elemental Composition of NiO/Activated Carbon

Element	Weight %	Atomic %	Weight % Error
C	72.31	54.98	10.55
Ni	8.66	2.001	0.48
Si	5.03	3.03	0.23
P	7.26	13.56	0.23
N	6.74	26.43	0.48
Total	100.00	100.00	

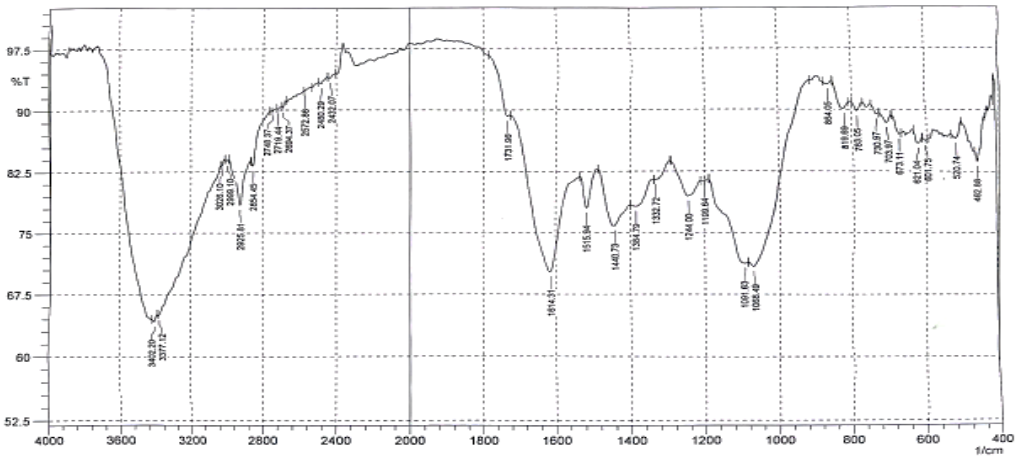

Fig. 8. FTIR Spectrum of Ficus carica Leaf

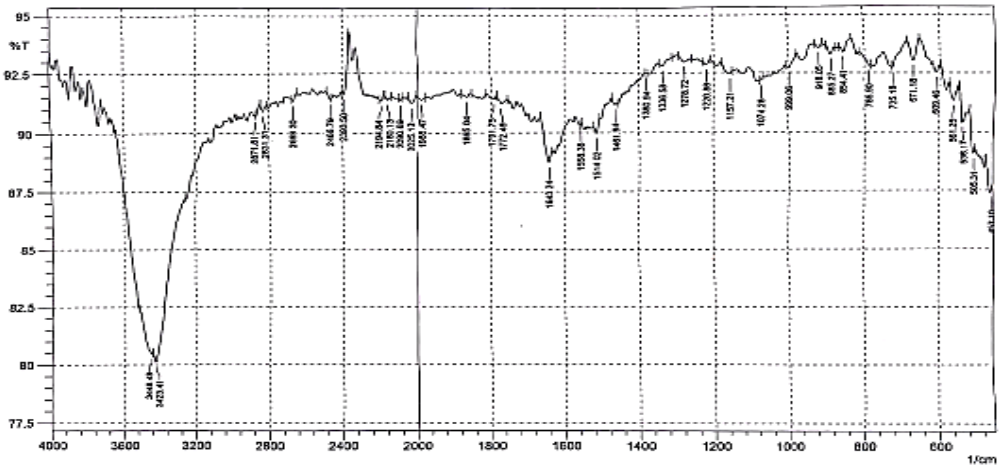

Fig. 9. FTIR Analysis for Activated Carbon

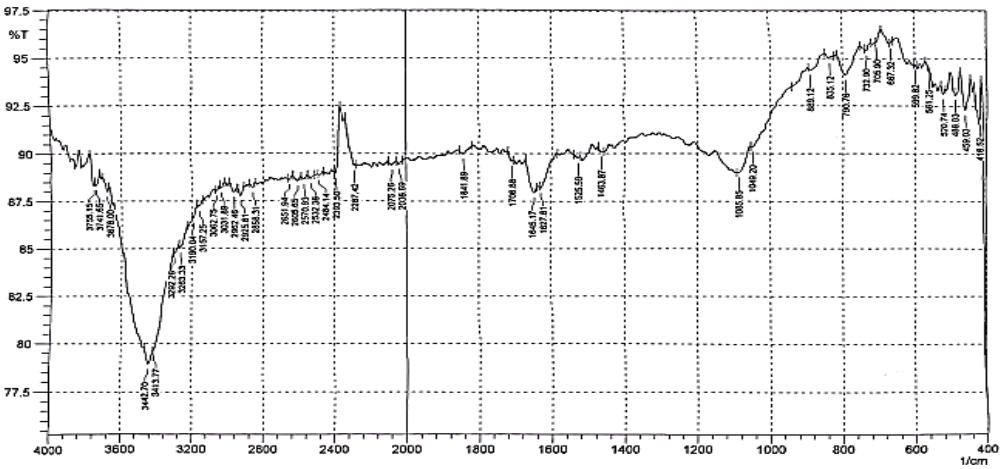

Fig. 10. FTIR for NiO/Activated Carbon

3.4. Experiments design

Batch experiments for the adsorption of malachite green using NiO nanoparticles, activated carbon (AC), and NiO/AC adsorbents were conducted with 50 ml of working material at room temperature and a continuous agitation speed of 200 rpm. a certain quantity of adsorbate (0.05-0.25) was introduced to various concentrations of MG solution samples (50-250 mg/L) at differing pH levels (4-10) and varying adsorption durations (30-240 min) the residual concentration of MG in each sample post-adsorption was quantified using UV-Visible absorption spectroscopy (Shimadzu AA1600, Japan) and the calibration curve shown in Fig. 1. The adsorption capacity and removal efficiency of MG by each adsorbent were determined using Eq. 1, Eq 2.

$$q_e = \frac{(C_o - C_e)V}{W} \quad (1)$$

$$RE\% = \frac{(C_o - C_e)}{C_o} \times 100\% \quad (2)$$

Where q_e is the adsorption capacity at equilibrium (mg/g), C_o and C_e are the initial and equilibrium concentrations of the cyanide (mg/L); V is the volume (L); W is the weight (g) of adsorbent, RE is the removal efficiency.

A DESIGN EXPERT (version 13 Stat-Ease) employing the RSM / I-Optimal method was used to design a series of experiments based on various independent variables, including MG concentration, pH, contact time, and adsorbent dosage, each assessed at five different levels. the independent variable along with its levels and the removal efficiency for various adsorbents is shown in Table 5 and Table 6.

Table 5. Experimental levels of independent variables in adsorption

Factor	Name	Units	Level 1	Level 2	Level 3	Level 4	Level 5
A	Conc.	mg/L	50	100	150	200	250
B	pH	pH	4	6	7	8	10
C	Time	Min	30	60	120	180	240
D	Dosage	gm/50 mL	0.05	0.1	0.15	0.2	0.25

3.5. Adsorption Process Optimization

The overall model for removal efficiency on the adsorbent can be described by the following quadratic Eq. 3;

$$Y = \beta_o + \sum_{i=1}^{4} \beta_i X_i + \sum_{i=1}^{4} \beta_{ii} X_i^2 + \sum_{1 \le i \le j}^{4} \beta_{ij} X_i X_j + \varepsilon \quad (3)$$

Where Y is model response of equation, X_i is independent factor, Ɛ is error of the model, intercept of model, β_o is intercept of model, $\beta_i, \beta_{ii}, \beta_{ij}$ are linear, quadric, and interaction coefficients [58].

The regression models for the removal efficiencies of malachite green, expressed in coded terms of the components using NiO, AC, and NiO/AC adsorbents, are formulated based on the general equation and analyzed through the analysis of variance (ANOVA) test, as presented in Eq. 4, 5, and 6, along with Table 7, Table 8, and Table 9.

$$RE1\%(pb) = 62.2148 + 0.0875A + 5.1132B + 0.1362C - 54.6812D - 0.0037AB + 0.00003AC + 0.2463AD + 0.0096BC - 0.3.6375BD - 0.1362CD - 0.00043A^2 - 0.2321B^2 - 0.00012C^2 + 152.6444D^2 \quad (4)$$

$$RE2\%(Cu) = 64.2272 + 0.08833A + 5.2235B + 0.1477C - 58.1257D + 2.77AB + 0.165AC + 0.2391AD - 0.01012BC + 3.609BD - 0.1425CD - 0.00043A^2 - 0.2358B^2 - 0.00014C^2 + 172.53332D^2 \quad (5)$$

$$RE1\%(Zn) = 64.1090 + 0.0915A + 5.9012B + 0.1378C - 71.9593D - 0.00342AB + 0.000029AC + 0.23879AD - 0.01065BC + 3.2830BD - 0.1105CD - 0.00045A^2 - 0.2786B^2 - 0.000115C^2 - 211.4688D^2 \quad (6)$$

The Tables indicate that the regression models for dye removal using NiO, AC, and NiO/AC showed satisfactory concordance with experimental data, as the difference between the adjusted R^2 and projected R^2 was below 0.2 [59].similarly, the models and their interacting variables for each term are significant ($P < 0.05$), indicating that each model can be refined to enhance the projected outcomes.

Fig. 11 - Fig. 12 illustrate response surface plots showing the removal effectiveness of malachite green by NiO, AC, and NiO/AC adsorbents. Fig. 11 (a, b, c) indicates that the removal efficiency was higher and showed modest variation across different concentrations and pH levels. the adsorption behavior of malachite green on NiO and NiO/AC is nearly identical, however it differs significantly for AC. this indicates that the influence of the nanomaterial adsorbent was dominant in the adsorption process of NiO and NiO/AC in comparison to AC. Consequently, the use of NiO nanoparticles on activated carbon diminished nanoparticle aggregation and enhanced malachite green adsorption. a similar trend was noted for the adsorption of malachite green on activated carbon derived from Ficus Carica leaves, including both metal and nonmetal oxides Fig. 12 (a, b, c) illustrates the relationship between adsorbent dose and adsorbate concentration. it was found that removal efficiency marginally increased with the increasing of adsorbent dose, reaching maximum removal efficiency at an adsorbent dose of 0.25 mg/50 ml and a malachite green concentration of 150 mg/L.

The removal effectiveness diminished as the concentration of malachite green increased. this means the adsorbent achieves saturation capacity at 150 mg/L, after which desorption dominates at higher concentrations.

similar results were achieved by [60]. Fig. 13 (a, b, c) illustrates the modification of the adsorbent dosage (0.05-0.25 mg/50ml) with the solution pH ranging from 4 to 10. It was noted that the removal effectiveness improved with both pH and adsorbent dosage, achieving maximum removal efficiency at 0.25 mg/50ml and pH 4. The removal efficiency diminished as pH increased. it means that the interaction is more pronounced at a pH of approximately 6, due to the rivalry between acidic H+ ions and dye cations for sorption sites, which reverses at elevated pH levels. Same results were observed for the adsorption of malachite green on rattan sawdust and acid-activated low-cost carbon [61, 62].

Table 6. Experimental runs generated by RSM with I-Optimal method

Run	A: Conc. (mg/L)	B: pH pH	C: Time (min)	D: Dosage (g/50mL)	RE1% (NiO)	RE2% (AC)	RE2% (NiO/AC)
1	250	6	240	0.2	94.6721	96.1773	98.4057
2	150	7	120	0.15	93.6906	98.1306	98.3751
3	150	7	120	0.15	93.6906	98.1306	98.3751
4	100	4	240	0.2	94.0412	97.8969	98.7433
5	50	10	240	0.25	93.6556	97.5464	98.0384
6	50	4	30	0.1	96.8453	85.247	98.688
7	100	4	180	0.05	94.0412	97.6701	98.7433
8	50	8	240	0.05	93.3401	98.6495	98.71
9	100	6	30	0.25	95.2164	98.1306	98.751
10	150	7	120	0.15	93.6906	98.8247	98.8367
11	150	4	120	0.25	97.9202	98.8932	99.9776
12	250	4	30	0.05	83.5256	77.3564	89.7019
13	250	10	240	0.05	97.0556	83.6594	96.867
14	100	6	30	0.25	95.969	98.8747	99.186
15	50	8	60	0.05	96.1443	95.5979	98.952
16	200	8	30	0.05	88.5205	87.118	92.9465
17	50	7	120	0.2	94.7422	97.2659	98.4793
18	250	4	30	0.2	89.0638	84.2926	93.517
19	100	10	30	0.15	97.7216	98.6669	99.608
20	250	10	120	0.25	96.3546	98.0185	99.172
21	150	10	240	0.15	96.1443	94.1098	98.52
22	250	10	30	0.15	90.9566	89.5133	94.5044
23	250	4	180	0.05	89.2741	87.5256	94.836
24	150	7	120	0.15	93.6906	98.7518	98.3751
25	50	7	120	0.2	94.7422	97.2555	98.4793

Table 7. ANOVA for the quadratic model of dye removal

Source	Sum of square	df	Mean square	F value	P value	
Model	261.29	14	18.66	73.74	< 0.0001	significant
A-Conc.	37.27	1	37.27	147.25	< 0.0001	
B-pH	19.85	1	19.85	78.43	< 0.0001	
C-Time	4.70	1	4.70	18.57	0.0015	
D-Dosage	19.45	1	19.45	76.83	< 0.0001	
AB	1.87	1	1.87	7.41	0.0215	
AC	62.44	1	62.44	246.73	< 0.0001	
AD	13.83	1	13.83	54.64	< 0.0001	
BC	0.0222	1	0.0222	0.0878	0.7731	
BD	6.80	1	6.80	26.88	0.0004	
CD	1.07	1	1.07	4.24	0.0664	
A^2	2.74	1	2.74	10.83	0.0081	
B^2	19.05	1	19.05	75.26	< 0.0001	
C^2	4.05	1	4.05	15.99	0.0025	
D^2	0.5841	1	0.5841	2.31	0.1597	
Adjusted R^2	0.9844					
Predicted R^2	0.9178					

Table 8. ANOVA for the quadratic model of dye removal

Source	Sum of square	df	Mean square	F value	P value	
Model	929.28	14	66.38	77.41	< 0.0001	significant
A-Conc.	95.33	1	95.33	111.17	< 0.0001	
B-pH	28.36	1	28.36	33.07	0.0002	
C-Time	61.60	1	61.60	71.83	< 0.0001	
D-Dosage	157.02	1	157.02	183.11	< 0.0001	
AB	8.55	1	8.55	9.97	0.0102	
AC	1.32	1	1.32	1.54	0.2430	
AD	47.93	1	47.93	55.89	< 0.0001	
BC	85.43	1	85.43	99.62	< 0.0001	
BD	6.50	1	6.50	7.58	0.0203	
CD	14.28	1	14.28	16.65	0.0022	
A^2	68.39	1	68.39	79.75	< 0.0001	
B^2	17.41	1	17.41	20.30	0.0011	
C^2	7.45	1	7.45	8.69	0.0146	
D^2	11.56	1	11.56	13.48	0.0043	
Adjusted R^2	0.9798					
Predicted R^2	0.9044					

Table 9. ANOVA for the quadratic model of dye removal on the surface

Source	Sum of square	df	Mean square	F value	P value	
Model	145.46	14	10.39	43.91	< 0.0001	significant
A-Conc.	27.52	1	27.52	116.32	< 0.0001	
B-pH	3.03	1	3.03	12.81	0.0050	
C-Time	10.24	1	10.24	43.29	< 0.0001	
D-Dosage	14.67	1	14.67	62.01	< 0.0001	
AB	0.0839	1	0.0839	0.3545	0.5648	
AC	18.13	1	18.13	76.62	< 0.0001	
AD	11.98	1	11.98	50.64	< 0.0001	
BC	1.06	1	1.06	4.50	0.0600	
BD	0.0025	1	0.0025	0.0106	0.9199	
CD	1.89	1	1.89	8.00	0.0179	
A^2	4.43	1	4.43	18.74	0.0015	
B^2	1.35	1	1.35	5.69	0.0382	
C^2	1.82	1	1.82	7.70	0.0196	
D^2	0.1523	1	0.1523	0.6436	0.4410	
Adjusted R^2	0.9879					
Predicted R^2	0.9205					

4- Adsorption isotherm model

The experimental and theoretical results for AC and NiO/AC were analyzed through the correlation between malachite green dye concentration and the adsorption capacity of activated carbon and composite adsorbents under equilibrium conditions. the Langmuir and Freundlich isotherm models were employed to determine the diffusion of the adsorbate from the liquid phase to the solid phase [63, 64]. The equilibrium conditions were established for an adsorption duration of 120 minutes, malachite green dye concentrations ranging from 50 to 250 mg/L, a pH of 4, and an adsorption dose of 0.25 g per 50 mL. The data fitting is illustrated in Fig. 14 and Fig. 15, and the isotherm model constants are given in Table 10. The coefficients of the Freundlich models for NiO nanoparticles, AC, and NiO/AC show superior fit compared to the Langmuir models. This means that malachite green adsorption linked to multilayer adsorption on the sorbent surface sites [65].

5- Adsorption kinetic models

To assess the mass transfer rate of the adsorption process, which includes residence time and the adsorbate at the solid-liquid interface, two adsorption kinetic models were used for a duration of 120 minutes, with malachite green dye concentrations ranging from 50 to 250 mg/L, at a pH of 4, and an adsorption dose of 0.25 g per 50 ml. to characterize the dye adsorption mechanism on composite activated carbon, adsorption rate constants were determined using pseudo-first order and second-order models, with data fitting illustrated in Fig. 16 and Fig. 17. The kinetics of the two model coefficients were

summarized in Table 11. The correlation coefficient R^2 was used to access the consistency between experimental data and model predictions; models with a higher R^2 are more effective in characterizing the adsorption kinetics. Compared to pseudo-first order, the results demonstrate that pseudo-second-order kinetics yields superior R^2 values. this indicates that the adsorption rate was inversely proportional to the square of the dye concentration during a chemical process affected by the interaction between adsorbate and adsorbent [66].

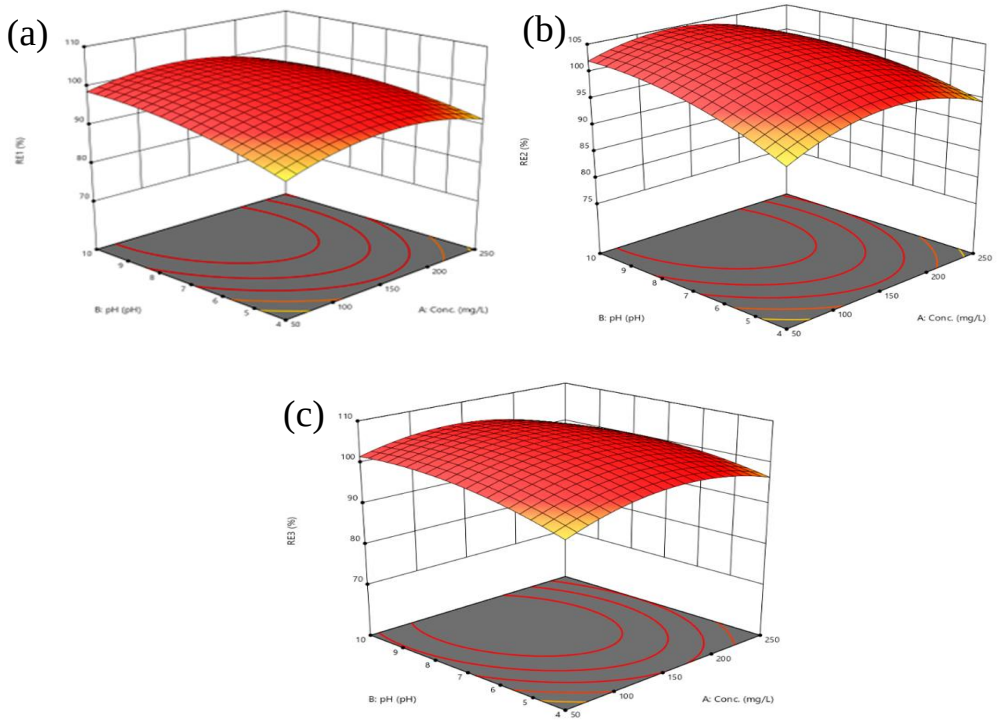

Fig. 11. (a, b, c). The effect of the initial concentration and pH for NiO, AC and NiO/AC

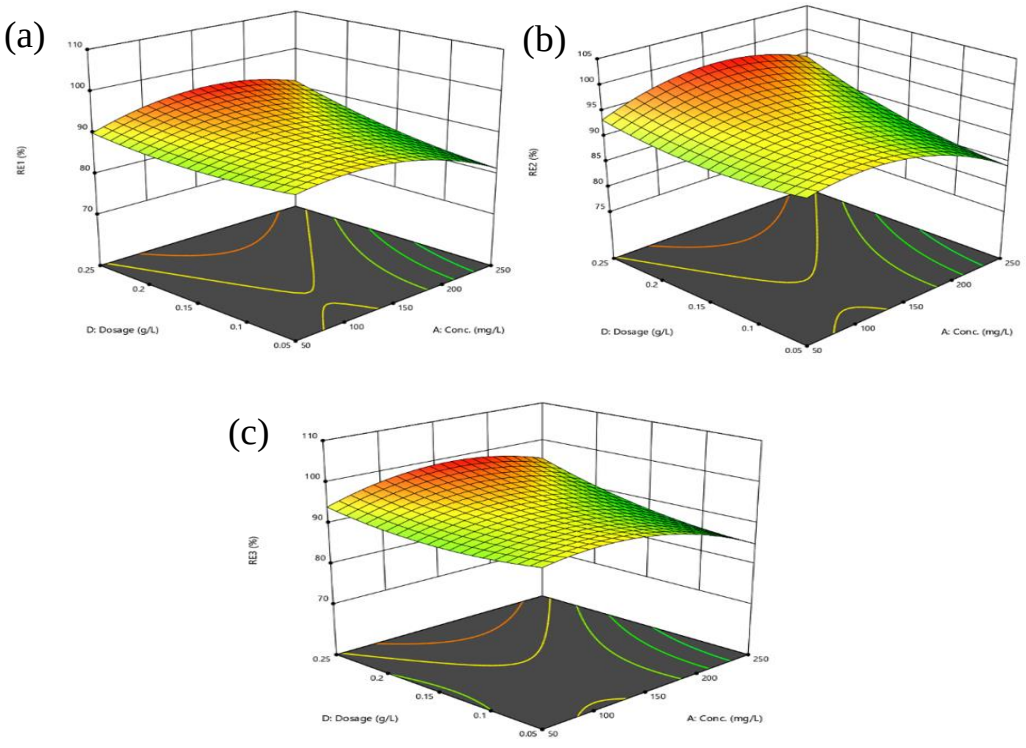

Fig. 12. The effect of the initial concentration and adsorbent dose for NiO, AC and NiO/AC

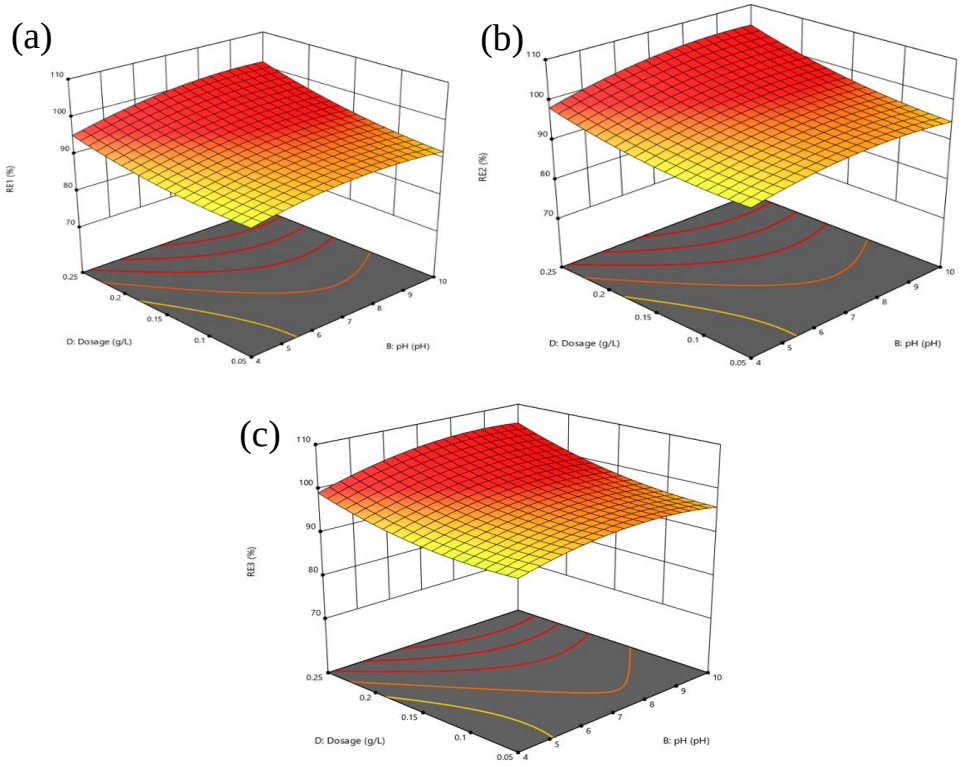

Fig. 13. The effect of the adsorbent dose and pH of solution NiO, AC and NiO/AC

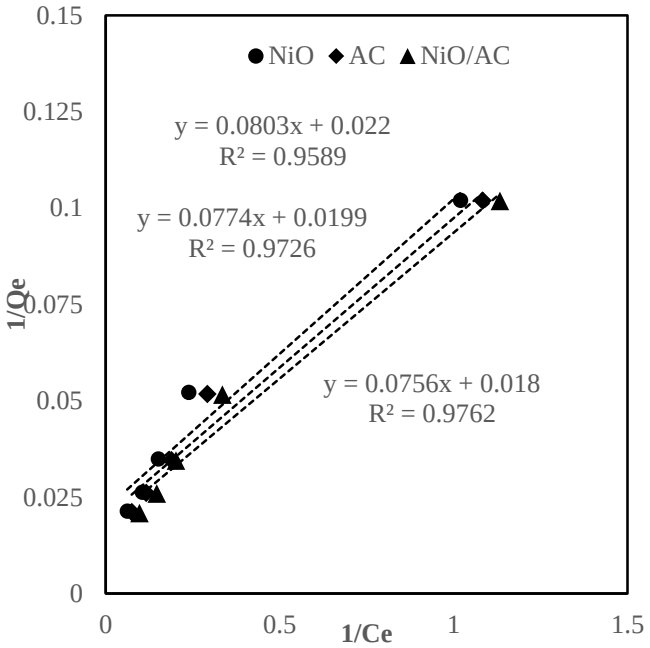

Fig. 14. adsorption Langmuir isotherm plots

Table 10. Coefficients of the adsorption isotherm model

	Langmuir			Freundlich		
	K_L (L/mg)	q_m (mg/g)	R^2	k_f (mg/g)	n	R^2
NIO	0.2738	45.451	0.9589	9.7030	1.7367	0.9931
AC	0.2570	50.2324	0.9725	2.7257	1.6553	0.9915
NIO/AC	0.2769	49.3971	0.97863	2.7516	1.5239	0.9921

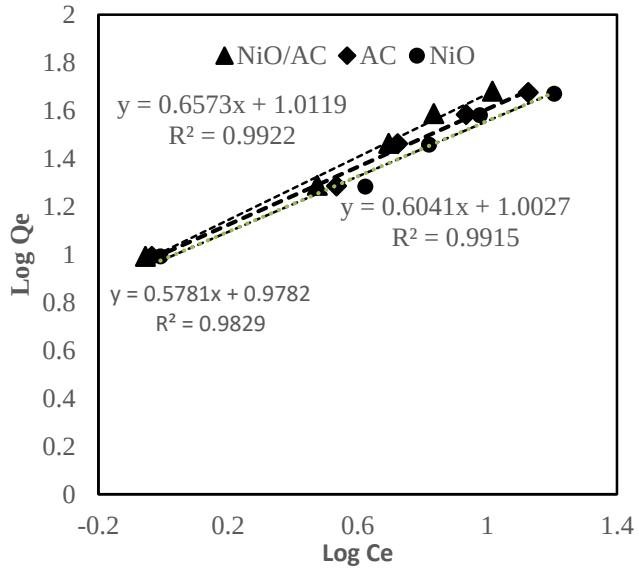

Fig. 15. Freundlich isotherm adsorption plots

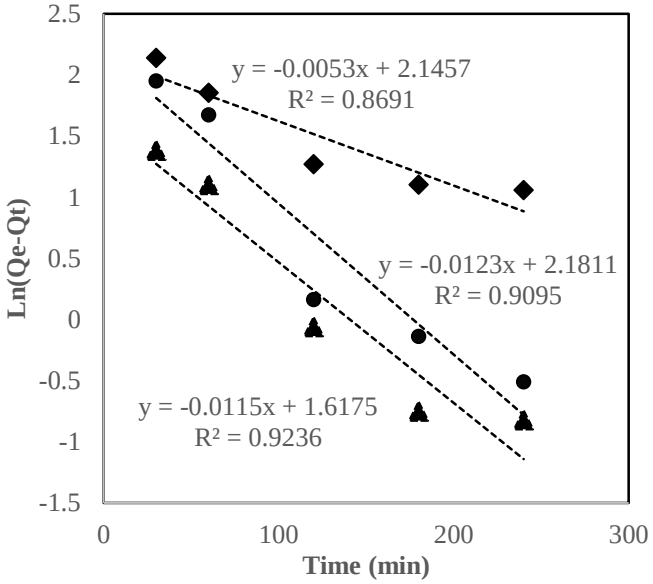

Fig. 16. Pseudo-first order plots

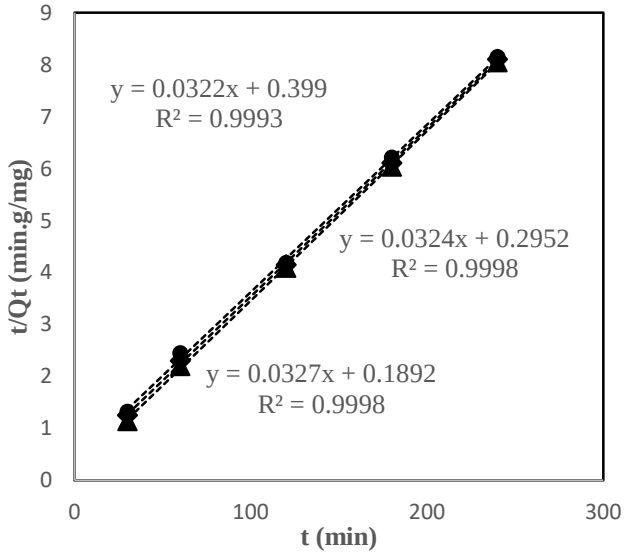

Fig. 17. Pseudo-second order plots

Table 11. adsorption kinetic model coefficients

	First Order			Second Order		
	k_1 (min^{-1})	qe (mg/g)	R^2	k_2 (min^{-1})	qe (mg/g)	R^2
NIO	0.01233	8.8561	0.9095	-0.0322	31.0222	0.9992
AC	0.0052	8.5480	0.8691	-0.0324	30.8519	0.99979
NIO/AC	0.0114	5.0405	0.9236	-0.0326	30.6209	0.9998

6- Conclusion

This research investigated the adsorption of malachite green from aqueous solution using Green NiO nanoparticles, activated carbon, and composite activated carbon adsorbents. Ficus carica leaf was used to prepare activated carbon by pyrolysis of carbonic acid with microwave technique, and Ficus carica leaf extract was used to synthesize NiO nanoparticles. the NiO nanoparticles, activated carbon, and NiO/AC were characterized by Brunauer-Emmett-Teller analysis, scanning electron microscopy with energy dispersive X-ray analysis, X-ray diffraction, and Fourier transform infrared spectroscopy.

The characterization results showed a high BET surface area of 961.6142 m^2/g for AC/NiO, due to the presence of NiO nanoparticles on the activated carbon surface. Design-Expert (13 Stat-Ease) software with Response Surface Methodology (RSM) was employed to analyze the effects of initial concentration, pH, contact time, and the doses of NiO, activated carbon (AC), and NiO/AC on malachite green removal efficiency. the maximum removal efficiencies were obtained at optimum conditions of pH 4, a contact time of 120 min, an adsorbent dosage of 0.25 g/50 mL, and a dye concentration of 150 mg/L. Adsorption isotherm and kinetic studies were conducted to determine the adsorption type and mechanism using the Langmuir and the Freundlich isotherm models, as well as pseudo-first- and second-order kinetic models. the results indicated that the Freundlich isotherm and pseudo-second-order kinetic models were the most effective in representing the equilibrium adsorption data for all types of adsorbents. Consequently, the adsorption process of malachite green on the NiO nanoparticles, activated carbon, and NiO/AC was chemosorption on multilayer surface sites.

Acknowledgment

The authors express their gratitude to the Biochemical Engineering Department of Al-Khwarizmi College of Engineering, University of Baghdad, for their assistance in conducting this research.

References

[1] G. Crini, "Non-conventional low-cost adsorbents for dye removal: A review," *Bioresource Technology*, vol. 97, no. 9, pp. 1061-1085, 2006, https://doi.org/10.1016/j.biortech.2005.05.001

[2] M. Abbas, M. Adil, S. Ehisham-ul-Haque, B. Munir, M. Yasmeen, A. Ghaffar, G.A. Shar, M. Asif Tahir, "Vibrio fischeri bioluminescence inhibition assay for ecotoxicity assessment: A review," *Science of The Total Environment*, vol. 626, pp. 1295-1309, 2018, https://doi.org/10.1016/j.scitotenv.2018.01.066

[3] S. De Gisi, G. Lofrano, M. Grassi, and M. Notarnicola, "Characteristics and adsorption capacities of low-cost sorbents for wastewater treatment: A review," *Sustainable Materials and Technologies*, vol. 9, pp. 10-40, 2016, https://doi.org/10.1016/j.susmat.2016.06.002

[4] J. Hashimoto, J. Paschoal, J. Queiroz, and F. Reyes, "Considerations on the Use of Malachite Green in Aquaculture and Analytical Aspects of Determining the Residues in Fish: A Review," *Journal of Aquatic Food Product Technology*, vol. 20, pp. 273-294, 2011 , https://doi.org/10.1080/10498850.2011.569643

[5] J. Sharma, S. Sharma, and V. Soni, "Toxicity of malachite green on plants and its phytoremediation: A review," *Regional Studies in Marine Science*, vol. 62, p. 102911, 2023, https://doi.org/10.1016/j.rsma.2023.102911

[6] K. Mohammadi, S. Khalesro, Y. Sohrabi, and G. Heidari, "A Review: Beneficial Effects of the Mycorrhizal Fungi for Plant Growth," *Journal of Applied Environment Biological Sciences*, vol. 1, pp. 310-319, 2011.

[7] H. N. J. Hoong and N. Ismail, "Removal of Dye in Wastewater by Adsorption-Coagulation Combined System with Hibiscus sabdariffa as the Coagulant," *MATEC Web Conference*, vol. 152, p. 01008, 2018. https://doi.org/10.1051/matecconf/201815201008

[8] P. V. Nidheesh, M. Zhou, and M. A. Oturan, "An overview on the removal of synthetic dyes from water by electrochemical advanced oxidation processes," *Chemosphere*, vol. 197, pp. 210-227, 2018, https://doi.org/10.1016/j.chemosphere.2017.12.195

[9] J. Sarasa, M. P. Roche, M. P. Ormad, E. Gimeno, A. Puig, and J. L. Ovelleiro, "Treatment of a wastewater resulting from dyes manufacturing with ozone and chemical coagulation," *Water Research*, vol. 32, no. 9, pp. 2721-2727, 1998, https://doi.org/10.1016/S0043-1354(98)00030-X

[10] A. E. Abdelhamid, A. E. Elsayed, M. Naguib, and E. A. Ali, "Effective Dye Removal by Acrylic-Based Membrane Constructed from Textile Fibers Waste," *Fibers and Polymers*, vol. 24, no. 7, pp. 2391-2399, 2023, https://doi.org/10.1007/s12221-023-00247-z

[11] S. Selvakumar, R. Manivasagan, and K. Chinnappan, "Biodegradation and decolourization of textile dye wastewater using Ganoderma lucidum," 3 *Biotech*, vol. 3, no. 1, pp. 71-79, Feb 2013, https://doi.org/10.1007/s13205-012-0073-5

[12] Removal of Malachite Green from Aqueous Solution using Ficus Benjamina Activated Carbon-Nonmetal Oxide synthesized by pyro Carbonic Acid Microwave," *Al-Khwarizmi Engineering Journal*, vol. 19, no. 2, pp. 26- 38, 2023, https://doi.org/10.22153/kej.2023.03.002

[13] K. E. Talib and S. D. Salman, "Removal of malachite green from aqueous solution using Ficus benjamina activated carbon-metal oxide synthesized by pyrocarbonic acid microwave," *Desalination and Water Treatment*, vol. 302, pp. 195-209, 2023, https://doi.org/10.5004/dwt.2023.29620

[14] Momina and K. Ahmad, "Feasibility of the adsorption as a process for its large scale adoption across industries for the treatment of wastewater: Research gaps and economic assessment," *Journal of Cleaner Production*, vol. 388, p. 136014, 2023, https://doi.org/10.1016/j.jclepro.2023.136014

[15] Y. Alhamed, "Activated Carbon from Date Stone by ZnCl2 Activation," *Journal of King Saud University Engineering Science*, vol. 17, 2006.

[16] O. Ioannidou and A. Zabaniotou, "Agricultural residues as precursors for activated carbon production—A review," *Renewable Sustainable Energy Reviews*, vol. 11, no. 9, pp. 1966-2005, 2007, https://doi.org/10.1016/j.rser.2006.03.013

[17] M. Ajmal, R. A. K. Rao, and M. A. Khan, "Adsorption of copper from aqueous solution on Brassica cumpestris (mustard oil cake)," *Journal of Hazardous Materials*, vol. 122, no. 1, pp. 177-183, 2005, https://doi.org/10.1016/j.jhazmat.2005.03.029

[18] H. Demiral and C. Güngör, "Adsorption of copper(II) from aqueous solutions on activated carbon prepared from grape bagasse," *Journal of Cleaner Production*, vol. 124, pp. 103-113, 2016, https://doi.org/10.1016/j.jclepro.2016.02.084

[19] R. Baccar, J. Bouzid, M. Feki, and A. Montiel, "Preparation of activated carbon from Tunisian olive-waste cakes and its application for adsorption of heavy metal ions," *Journal of Hazardous Materials*, vol. 162, no. 2, pp. 1522-1529, 2009, https://doi.org/10.1016/j.jhazmat.2008.06.041

[20] N. Fiol, I. Villaescusa, M. Martínez, N. Miralles, J. Poch, and J. Serarols, "Sorption of Pb(II), Ni(II), Cu(II) and Cd(II) from aqueous solution by olive stone waste," *Separation and Purification Technology*, vol. 50, no. 1, pp. 132-140, 2006, https://doi.org/10.1016/j.seppur.2005.11.016

[21] A.-N. A. El-Hendawy, A. J. Alexander, R. J. Andrews, and G. Forrest, "Effects of activation schemes on porous, surface and thermal properties of activated carbons prepared from cotton stalks," *Journal of Analytical and Applied Pyrolysis*, vol. 82, no. 2, pp. 272-278, 2008, https://doi.org/10.1016/j.jaap.2008.04.006

[22] J. M. V. Nabais, C. E. C. Laginhas, P. J. M. Carrott, and M. M. L. Ribeiro Carrott, "Production of activated carbons from almond shell," *Fuel Processing Technology*, vol. 92, no. 2, pp. 234-240, 2011, https://doi.org/10.1016/j.fuproc.2010.03.024

[23] Q. Cao, K.-C. Xie, Y.-K. Lv, and W.-R. Bao, "Process effects on activated carbon with large specific surface area from corn cob," *Bioresource Technology*, vol. 97, no. 1, pp. 110-115, 2006, https://doi.org/10.1016/j.biortech.2005.02.026

[24] B. M. W. P. K. Amarasinghe and R. A. Williams, "Tea waste as a low cost adsorbent for the removal of Cu and Pb from wastewater," *Chemical Engineering Journal*, vol. 132, no. 1, pp. 299-309, 2007, https://doi.org/10.1016/j.cej.2007.01.016

[25] S. Erdoğan, Y. Önal, C. Akmil-Başar, S. Bilmez-Erdemoğlu, Ç. Sarıcı-Özdemir, E. Köseoğlu, G. İçduygu ﷺ, "Optimization of nickel adsorption from aqueous solution by using activated carbon prepared from waste apricot by chemical activation," *Applied Surface Science*, vol. 252, no. 5, pp. 1324-1331, 2005, https://doi.org/10.1016/j.apsusc.2005.02.089

[26] Y.-z. Cui and M.-c. Tian, "Three-dimensional numerical simulation of thermal-hydraulic performance of a circular tube with edgefold-twisted-tape inserts," *Journal of Hydrodynamics*, vol. 22, no. 5, pp. 662-670, 2010, https://doi.org/10.1016/s1001-6058(09)60101-3

[27] C. J. Durán-Valle, M. Gómez-Corzo, V. Gómez-Serrano, J. Pastor-Villegas, and M. L. Rojas-Cervantes, "Preparation of charcoal from cherry stones," *Applied Surface Science*, vol. 252, no. 17, pp. 5957-5960, 2006, https://doi.org/10.1016/j.apsusc.2005.11.004

[28] R. M. Suzuki, A. D. Andrade, J. C. Sousa, and M. C. Rollemberg, "Preparation and characterization of activated carbon from rice bran," *Bioresource Technology*, vol. 98, no. 10, pp. 1985-1991, 2007, https://doi.org/10.1016/j.biortech.2006.08.001

[29] T. C. Chandra, M. M. Mirna, J. Sunarso, Y. Sudaryanto, and S. Ismadji, "Activated carbon from durian shell: Preparation and characterization," *Journal of the Taiwan Institute of Chemical Engineers*, vol. 40, no. 4, pp. 457-462, 2009/07/01/ 2009, https://doi.org/10.1016/j.jtice.2008.10.002

[30] Khatab E. Talib and S. D. Salman, "Removal of Malachite Green from Aqueous Solution using Ficus Benjamina Activated Carbon-Metal Oxide synthesized by pyro carbonic acid microwave," *Desalination and Water Treatment*, vol. 302, no. August 2023, pp. 105-209, 2023, https://doi.org/10.5004/dwt.2023.29620

[31] N. Rani, P. Singh, S. Kumar, P. Kumar, V. Bhankar, and K. Kumar, "Plant-mediated synthesis of nanoparticles and their applications: A review," *Materials Research Bulletin*, vol. 163, p. 112233, 2023, https://doi.org/10.1016/j.materresbull.2023.112233

[32] M. A. Rahman, R. Radhakrishnan, and R. Gopalakrishnan, "Structural, optical, magnetic and antibacterial properties of Nd doped NiO nanoparticles prepared by co-precipitation method," *Journal of Alloys and Compounds*, vol. 742, pp. 421-429, 2018, https://doi.org/10.1016/j.jallcom.2018.01.298

[33] F. L. Jia, L. Z. Zhang, X. Y. Shang, and Y. Yang, "Non-Aqueous Sol–Gel Approach towards the Controllable Synthesis of Nickel Nanospheres, Nanowires, and Nanoflowers," *Advanced Material*, vol. 20, no. 5, pp. 1050-1054, 2008, https://doi.org/10.1002/adma.200702159

[34] B. Nagaraj, N. B. Krishnamurthy, P. Liny, and R. DivyaTkAndDinesh, "Biosynthesis of Gold Nanoparticles of Ixora Coccinea Flower Extract & Their Antimicrobial Activities," *International journal of pharma and bio sciences*, 2011.

[35] A. E. Ferenji, Y. E. Hassen, S. L. Mekuria, and W. M. Girma, "Biogenic mediated green synthesis of NiO nanoparticles for adsorptive removal of lead from aqueous solution," *Heliyon*, vol. 10, no. 11, p. e31669, 2024, https://doi.org/10.1016/j.heliyon.2024.e31669

[36] C. J. Pandian, R. Palanivel, and S. Dhananasekaran, "Green synthesis of nickel nanoparticles using Ocimum sanctum and their application in dye and pollutant adsorption," *Chinese Journal of Chemical Engineering*, vol. 23, no. 8, pp. 1307-1315, 2015, https://doi.org/10.1016/j.cjche.2015.05.012

[37] S. Hussain, M. A. Muazzam, M. Ahmed, M. Ahmad, Z. Mustafa, S. Murtaza, J. Ali, M. Ibrar, M. Shahid, M. Imran, "Green synthesis of nickel oxide nanoparticles using Acacia nilotica leaf extracts and investigation of their electrochemical and biological properties," *Journal of Taibah University for Science*, vol. 17, no. 1, p. 2170162, 2023, https://doi.org/10.1080/16583655.2023.2170162

[38] A. Kiran, S. Hussain, I. Ahmad, M. Imran, M. Saqib, B. Parveen, K. S. Munawar, W. Mnif, M. Al Huwayz, N. Alwadai, M. Iqbal, "Green synthesis of NiO and NiO@graphene oxide nanomaterials using Elettaria cardamomum leaves: Structural and electrochemical studies," *Heliyon*, vol. 10, no. 20, p. e38613, 2024, https://doi.org/10.1016/j.heliyon.2024.e38613

[39] H. G. Gebretinsae, M. G. Tsegay, and Z. Y. Nuru, "Biosynthesis of nickel oxide (NiO) nanoparticles from cactus plant extract," *Materials Today: Proceedings*, vol. 36, pp. 566-570, 2021, https://doi.org/10.1016/j.matpr.2020.05.331

[40] S. Prabhu, T. Daniel Thangadurai, P. Vijai Bharathy, and P. Kalugasalam, "Synthesis and characterization of nickel oxide nanoparticles using Clitoria ternatea flower extract: Photocatalytic dye degradation under sunlight and antibacterial activity applications," *Results in Chemistry*, vol. 4, p. 100285, 2022, https://doi.org/10.1016/j.rechem.2022.100285

[41] M. I. Din, A. G. Nabi, A. Rani, A. Aihetasham, and M. Mukhtar, "Single step green synthesis of stable nickel and nickel oxide nanoparticles from Calotropis gigantea: Catalytic and antimicrobial potentials," *Environmental Nanotechnology, Monitoring & Management*, vol. 9, pp. 29-36, 2018, https://doi.org/10.1016/j.enmm.2017.11.005

[42] B. T. Sone, X. G. Fuku, and M. Maaza, "Physical & Electrochemical Properties of Green Synthesized Bunsenite NiO Nanoparticles via Callistemon Viminalis' Extracts," *International Journal of Electrochemical Science*, vol. 11, no. 10, pp. 8204-8220, 2016, https://doi.org/10.20964/2016.10.17

[43] J. Iqbal, B. Abbasi, T. Mahmood, S. Hameed, A. Munir, and S. Kanwal, "Green synthesis and characterizations of Nickel oxide nanoparticles using leaf extract of Rhamnus virgata and their potential biological applications," *Applied Organometallic Chemistry*, 2019, https://doi.org/10.1002/aoc.4950

[44] Z. Sabouri et al., "Plant-based synthesis of NiO nanoparticles using salvia macrosiphon Boiss extract and examination of their water treatment," *Rare Metals*, vol. 39, no. 10, pp. 1134-1144, 2020, https://doi.org/10.1007/s12598-019-01333-z

[45] S. N. Shintre, S. Wadhai, and P. Thakur, "Synthesis of Ag/ZnO-AC composite photocatalyst: spectroscopic investigation, parameter optimization, synergistic effect and performance enhancement for cost-effective photocatalytic degradation of phenols and dyes," *Water Science and Technology*, vol. 85, no. 9, pp. 2663-2681, 2022, htpps://doi.org/10.2166/wst.2022.137

[46] A. Jain, M. Michalska, A. Zaszczyńska, and P. Denis, "Surface modification of activated carbon with silver nanoparticles for electrochemical double layer capacitors," *Journal of Energy Storage*, vol. 54, p. 105367, 2022, https://doi.org/10.1016/j.est.2022.105367

[47] Ç. d. Şentorun-Shalaby, M. G. Uçak-Astarlıogˇlu, L. Artok, and Ç. Sarıcı, "Preparation and characterization of activated carbons by one-step steam pyrolysis/activation from apricot stones," *Microporous and Mesoporous Materials*, vol. 88, no. 1, pp. 126-134, 2006, https://doi.org/10.1016/j.micromeso.2005.09.003

[48] A. A. Al. Swat, T. A. Saleh, S. A. Ganiyu, M. N. Siddiqui, and K. R. Alhooshani, "Preparation of activated carbon, zinc oxide and nickel oxide composites for potential application in the desulfurization of model diesel fuels," *Journal of Analytical and Applied Pyrolysis*, vol. 128, pp. 246-256, 2017, https://doi.org/10.1016/j.jaap.2017.10.004

[49] S. D. Salman, I. M. Rasheed, and M. M. Ismaeel, "Removal of diclofenac from aqueous solution on apricot seeds activated carbon synthesized by pyro carbonic acid microwave," *Chemical Data Collections*, vol. 43, p. 100982, 2023, https://doi.org/10.1016/j.cdc.2022.100982

[50] W. Salah, W. Djeridi, A. Houas, and L. Elsellami, "Synergy between activated carbon and ZnO: a powerful combination for selective adsorption and photocatalytic degradation," *Materials Advances*, 2024, https://doi.org/10.1039/D3MA01171B

[51] A. Nasrullah, H. Khan, A. S. Khan, Z. Man, N. Muhammad, M. I. Khan, and N. M. Abd El-Salam,, "Potential biosorbent derived from Calligonum polygonoides for removal of methylene blue dye from aqueous solution," *Scientific World Journal*, vol. 2015, p. 562693, 2015, https://doi.org/10.1155/2015/562693

[52] P. Khare and B. P. Baruah, "Structural Parameters of Perhydrous Indian Coals," *International Journal of Coal Preparation and Utilization*, vol. 30, no. 1, pp. 44-67, 2010, https://doi.org/10.1080/19392691003781616

[53] Ş. Taşar, F. Kaya, and A. Özer, "Biosorption of lead(II) ions from aqueous solution by peanut shells: Equilibrium, thermodynamic and kinetic studies," *Journal of Environmental Chemical Engineering*, vol. 2, no. 2, pp. 1018-1026, 2014, https://doi.org/10.1016/j.jece.2014.03.015

[54] T. Benzaoui, A. Selatnia, and D. Djabali, "Adsorption of coper (II) ions from aqueous solution using bottom ash of expired drugs incineration," *Adsorption Science & Technology*, vol. 36, no. 1-2, pp. 114-129, 2018. https://doi.org/10.1177/0263617416685099

[55] R. Labied, O. Benturki, A. Y. Eddine Hamitouche, and A. Donnot, "Adsorption of hexavalent chromium by activated carbon obtained from a waste lignocellulosic material (Ziziphus jujuba cores): Kinetic, equilibrium, and thermodynamic study," *Adsorption Science & Technology*, vol. 36, no. 3-4, pp. 1066-1099, 2018, https://doi.org/10.1177/0263617417750739

[56] Freeman, I. J., Salmon, J. L., & Coburn, J. Q. "CAD Integration in Virtual Reality Design Reviews for Improved Engineering Model Interaction", *In ASME 2016 International Mechanical Engineering Congress & Exposition*, 2016, https://doi.org/10.1115/IMECE2016-66948

[57] S. Ilyas, H. Heryanto, and D. Tahir, "Correlation between structural and optical properties of CuO/carbon nanoparticle in supports the photocatalytic performance and attenuate the electromagnetic wave," *Journal of Environmental Chemical Engineering*, vol. 9, no. 1, p. 104670, 2021, https://doi.org/10.1016/j.jece.2020.104670

[58] S. Saini, J. Chawla, R. Kumar, and I. Kaur, "Response surface methodology (RSM) for optimization of cadmium ions adsorption using C16-6-16 incorporated mesoporous MCM-41," *SN Applied Sciences*, vol. 1, 2019, https://doi.org/10.1007/s42452-019-0922-5

[59] DESIGN EXPERT 13. Stat-Ease Inc.

[60] B. H. Hameed and M. I. El-Khaiary, "Batch removal of malachite green from aqueous solutions by adsorption on oil palm trunk fibre: Equilibrium isotherms and kinetic studies," *Journal of Hazardous Materials*, vol. 154, no. 1, pp. 237-244, 2008, https://doi.org/10.1016/j.jhazmat.2007.10.017

[61] B. H. Hameed and M. I. El-Khaiary, "Malachite green adsorption by rattan sawdust: Isotherm, kinetic and mechanism modeling," *Journal of Hazardous Materials*, vol. 159, no. 2, pp. 574-579, 2008, https://doi.org/10.1016/j.jhazmat.2008.02.054

[62] M. Hema and S. Arivoli, "Adsorption kinetics and thermodynamics of malachite green dye unto acid activated low cost carbon," *Journal of applied sciences and environmental management*, vol. 12, no. 1, 2008, https://doi.org/10.4314/jasem.v12i1.55568

[63] A. E. Nemr, "Potential of pomegranate husk carbon for Cr(VI) removal from wastewater: Kinetic and isotherm studies," *Journal of Hazardous Material*, vol. 161, no. 1, pp. 132-141, 2009, https://doi.org/10.1016/j.jhazmat.2008.03.093

[64] X.-E. Shen, X.-Q. Shan, D.-M. Dong, X.-Y. Hua, and G. Owens, "Kinetics and thermodynamics of sorption of nitroaromatic compounds to as-grown and oxidized multiwalled carbon nanotubes," *Journal of Colloid and Interface Science*, vol. 330, no. 1, pp. 1-8, 2009, https://doi.org/10.1016/j.jcis.2008.10.023

[65] A. Behnamfard and M. M. Salarirad, "Equilibrium and kinetic studies on free cyanide adsorption from aqueous solution by activated carbon," *Journal of Hazardous Materials*, vol. 170, no. 1, pp. 127-133, 2009, https://doi.org/10.1016/j.jhazmat.2009.04.124

[66] T. Farías, L. C. de Ménorval, J. Zajac, and A. Rivera, "Benzalkonium chloride and sulfamethoxazole adsorption onto natural clinoptilolite: effect of time, ionic strength, pH and temperature," *Journal of Colloid and Interface Science*, vol. 363, no. 2, pp. 465-475, 2011, https://doi.org/10.1016/j.jcis.2011.07.067

التخليق الأخضر لجسيمات أكسيد النيكل النانوية مع الكاربون المنشط من أوراق نبات التين ومستخلصة لإزالة المالاكيت الأخضر

رغد محمد هادي [١،*]، سامي داود سلمان [١]

١ قسم هندسة الكيمياء الأحيائية، كلية الهندسة الخوارزمي، جامعة بغداد، بغداد ٤٧٠٢٤، العراق

الخلاصة

استحوذت عملية التخليق الأخضر للجسيمات النانوية والكاربون المنشط على اهتمام الباحثين لما تتميز به من سرعة وكفاءة من حيث التكلفة، الاستدامة وكونها صديقة للبيئة. تتناول هذه الورقة البحثية تخليق الكاربون المنشط (AC) وجسيمات أكسيد النيكل النانوية (NiO–NPs) من أوراق التين ومستخلصاتها لإزالة صبغة المالاكيت الخضراء من المحاليل المائية. تم أنتاج الكربون المنشط (AC) من أوراق التين باستخدام تقنية حامض البايروكربونيك والمايكرويف، بينما تم إنتاج جسيمات أكسيد النيكل النانوية باستخدام مستخلصات الأوراق كعامل مختزل. تم توصيف الكاربون المنشط المُصنّع وجسيمات أكسيد النيكل النانوية باستخدام تحليل بروناور– إيميت – تيلر، والمجهر الإلكتروني الماسح مع تحليل الأشعة السينية المشتتة للطاقة، وحيود الأشعة السينية، ومطيافية الأشعة تحت الحمراء بتحويل فوريه. تم فحص تأثير العوامل المختلفة، بما في ذلك تركيز صبغة المالاكيت الخضراء، ودرجة الحموضة، ووقت التلامس، وجرعات NiO و AC وNiO/AC، من خلال تطبيق منهجية استجابة السطح، باستخدام Design–Expert (13 Stat–Ease)

تم تحديد العوامل المثلى لتحقيق أقصى كفاءة إزالة لصبغة المالاكيت الخضراء لتكون بتركيز أوليً قدره ١٥٠ مجم/لتر، ودرجة حموضة ٤، وفترة تلامس ١٢٠ دقيقة، وجرعة امتزاز قدرها ٠,٢٥ غم/لتر، مما أعطى كفاءة إزالة قدرها ٩٧,٩٢٠٢%، ٩٨,٨٩٣٢% و ٩٩,٩٧٧٦%، على التوالي.

تم تحليل بيانات الامتزاز عند الاتزان وفقًا لنماذج لانغمويز وفروينديلش المتساوية الحرارة، بالإضافة إلى النماذج الحركية الزائفة من الدرجة الأولى والثانية. وقد أشارت النتائج إلى أن نموذج فروندليش المتساوي الحرارة والنماذج الحركية الزائفة من الدرجة الثانية كانت الأكثر تأثيرا في تمثيل بيانات الامتزاز.

الكلمات الدالة: اوراق نبات التين، الجسيمات النانوية، الكاربون المنشط، المالاكيت الاخضر.